Enhanced electrochemical performance of vanadium carbide MXene composites for supercapacitors

Cite as: APL Mater. 10, 060901 (2022); doi: 10.1063/5.0087457
Submitted: 6 February 2022 • Accepted: 10 May 2022 •
Published Online: 1 June 2022

Syedah Afsheen Zahra,[1,2] Babak Anasori,[2] Muhammad Z. Iqbal,[3] Florent Ravaux,[4] Mohammednoor Al Tarawneh,[3] and Syed Rizwan[1,a)]

AFFILIATIONS

[1] Physics Characterization and Simulations Lab (PCSL), Department of Physics, School of Natural Sciences (SNS), National University of Sciences and Technology (NUST), Islamabad 44000, Pakistan
[2] Department of Mechanical and Energy Engineering, Purdue School of Engineering and Technology, Indiana University-Purdue University Indianapolis, Indianapolis, Indiana 46202, USA
[3] Department of Chemical and Petroleum Engineering, United Arab Emirates University, P.O. Box 15551, Al-Ain, United Arab Emirates
[4] Department of Physics, Khalifa University, Abu Dhabi, United Arab Emirates

Note: This paper is part of the Special Topic on Materials Challenges for Supercapacitors.
[a)] **Author to whom correspondence should be addressed:** syedrizwan@sns.nust.edu.pk and syedrizwanh83@gmail.com.
Tel: 0092 51 886 5599.

ABSTRACT

Two-dimensional (2D) surface-terminated layered transition metal carbide MXenes with high electrochemical performance paved the way for robust energy storage supercapacitor devices. However, because of the 2D nature of the MXene flakes, self-restacking of 2D MXene flakes limits the use of all the flake functionalized surfaces in MXene electrodes. Here, we report the synthesis of V_2CT_x MXene and multiwall carbon nanotube (MWCNT)/V_2CT_x composites as a promising electrode material for hybrid energy storage devices. Our hybrid electrodes exhibited enhanced electrochemical performance and a gravimetric capacitance of 1842 F g^{-1} at a scan rate of 2 mV s^{-1}, with a specific charge capacity of 62.5 A h/g. Moreover, the electrodes presented an excellent rate performance, durability, and retention capacity of 94% lasted up to 10 000 cycles. Density functional theory calculations provided electronic and structural properties of the considered MWCNT@V_2CT_x. Therefore, the introduction of MWCNTs enhanced the conductivity and reaction kinetics of the MXenes and facilitates the charge storage mechanism useful for next-generation smart energy storage devices.

I. INTRODUCTION

Owing to the continuous technological advancement and increased fuel waste emission causing serious environmental concerns, the demand for the development of eco-friendly, efficient, and clean energy harvesting storage devices is increasing.[1] In recent years, the production of wearable electronics, a proliferation of portable devices, and a widespread electrical automobile industry accelerated the energy demand. The current research in the field focuses on the management of green energy production and consumption, but the rapid growth in the population demands safe and low-cost energy storage devices for the next generation of smart electric grids. The electrochemical energy storage devices attracted much attention due to their high energy and power densities along with high durability.[2–4] The high gravimetric energy density (260 W h kg^{-1}) and long-life cyclability of Li-ion batteries made them the most suitable candidate for energy storage devices. However, nonuniform global distribution and shortage of Li resources require smart resource management.[5] Therefore, scientists are looking for alternative energy storage systems for the miniaturization of microelectronics and the emerging internet of things for different energy applications.[6] In this scenario, supercapacitors emerge as

promising alternatives to rechargeable batteries for their high-power delivery and rapid energy harvesting due to the fast electron-ion kinetics and long-life cycle.[7–12]

Electrodes and electrolytes are two key factors that determine the performance of supercapacitors. The reaction kinetics are highly dependent upon the intrinsic properties of the electrode material, and hence, the footsteps to the discovery of new electrode materials never stopped.[13–18] In 2011, a new family of two-dimensional (2D) materials, namely, MXenes, was discovered at Drexel University, and it exhibited excellent electrochemical performance to be the promising candidate for energy harvesting/storage devices. Titanium carbide was the first of the series that was made by acidic selective etching of Al layers from the Ti_3AlC_2 MAX phase[19] and has remained as the most studied MXenes.[20] MAX phases are ternary carbides and nitrides with the general formula of $M_{n+1}AX_n$, re-discovered and expanded by Barsoum,[21–25] where M represents the transition metal, A is an element from group III or IV, while X is either carbon or nitrogen and n ranges from 1 to 4.[21,26–28] The mechanical exfoliation of the A-element layers is more challenging,[29] while selective etching of the A-group layers using suitable chemicals can lead to the formation of a stable 2D $M_{n+1}X_nT_x$ layered structure; where T_x represents surface terminations (–OH, –F, or =O attached to M atoms after the removal of the A atoms).[30–32] Similar to the MAX phase precursor, n = 1–4 in MXenes, giving the possibility of M_2X, M_3X_2, M_4X_3, and M_5X_4, such as V_2C, Ti_3C_2, Nb_3C_4, and Mo_4VC_4. Owing to the unique physicochemical properties of MXenes, such as hydrophilicity, high electrical conductivity, tunable optical properties, functionalized and tunable surface chemistry, and thermal and plasmonic properties, MXenes have been used in various applications, such as energy storage devices, electromagnetic interference (EMI) shielding,[33] catalysis,[34] electromagnetism, resistive random access memory devices (RRAMs),[35] and sensors, to name a few.[36–44]

Density function theory (DFT) studies have suggested that V_2CT_x MXene is one of the suitable materials for energy storage devices, such as Li-ion batteries and supercapacitors.[45,46] Being one of the thinnest members of the large family of MXenes, vanadium carbide with relatively high electrical conductivity (3300 S cm^{-1}),[50] and electrochemical properties having a pseudocapacitive functionalized surface, has grabbed much research attention. Along the same line of inquiry, Zhan *et al.*[51] explored pseudocapacitive performance for various $M_{n+1}X_nT_x$ structures in the aqueous H_2SO_4 electrolyte. Similarly, DFT computations established a correlation between Faradaic voltage windows of MXene electrodes and charge transfer descriptors.[52] Based on the total energies from DFT calculations and thermodynamic formalisms, charge–discharge curves of various MXene configurations were also attained.[53]

Few experimental studies were carried out in the past to investigate the properties of V_2CT_x MXene for its effective use in Li-, Na-, and Zn-ion batteries and micro-capacitors.[2,47–49,54] Different nanomaterials, such as carbon nanotubes (CNTs), have been used as a spacer to create a more open structure and, hence, increase the electrical conductivity and electrochemical stability. Previous studies showed that the addition of CNTs to MXene flakes increases the charge storage as well as rate performance. Xie *et al.* reported that the $Ti_3C_2T_x$/CNT film, made from self-assembly of CNTs and $Ti_3C_2T_x$, exhibits a high volumetric capacity of 421 mA h cm^{-3} at 20 mA g^{-1}.[55] Zhao *et al.* showed that the sandwich-like structure of the $Ti_3C_2T_x$/CNTs composite is stable even after 10 000 cycles.[59] Inspired by these studies and the above-mentioned manifested properties of V_2CT_x MXene, we have prepared multiwall carbon nanotube (MWCNT) composites with the V_2CT_x MXene powder to stabilize the MXene structure and provide additional conductive pathways, which can improve charge–discharge capacity. An excellent charge storage capacity of ~2400 F g^{-1}, enhanced storage retention, and stability are observed in the presented structure with a specific charge capacity of 57.407 A h g^{-1}.

II. RESULTS AND DISCUSSIONS

We first characterized the as received V_2AlC MAX phase powder using x-ray diffraction (XRD). Figure 1(a) represents the XRD pattern of the V_2AlC MAX phase with peaks at 13.4°, 35.5°, 36.2°, 41.2°, 45.3, 55.5°, and 63.8°, which matched the previously reported V_2AlC (JCPDS No. 29-0101). Our XRD result does not show any impurity phase peaks. After acidic selective etching with 50% HF (hydrofluoric acid) for 72 h, the (002) peak shifts toward a lower 2Θ of 8.9°, corresponding to a d-spacing of 9.9 Å [Fig. 1(b)]. The presence of a small peak at around 13.4° and 41.2° represents a small

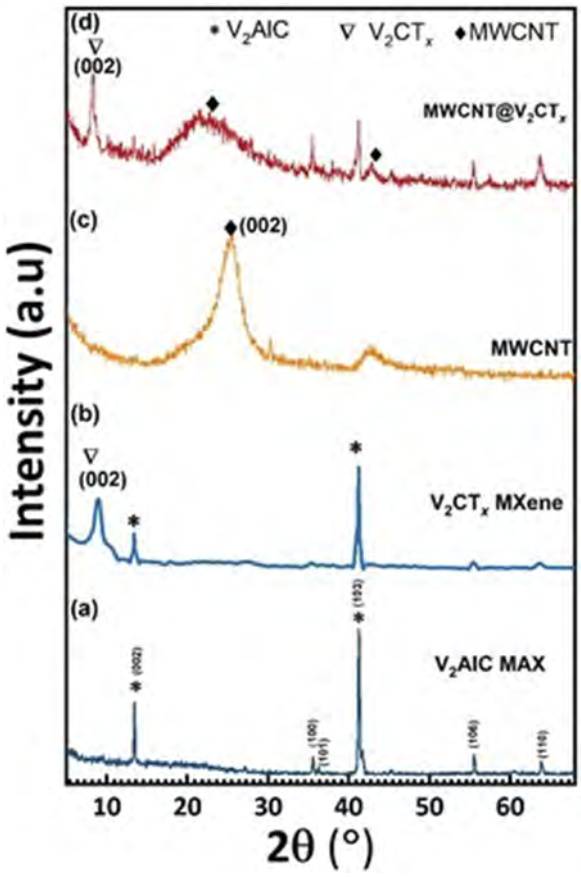

FIG. 1. XRD patterns of (a) the V_2AlC MAX phase, (b) V_2CT_x MXene after HF treatment, (c) Multiwall Carbon Nanotubes (MWCNTs), and (d) MWCNT@V_2CT_x.

amount of the unetched MAX phase, which is in good agreement with the previous studies.[56]

The as-synthesized multilayered (ML) V_2CT_x MXene was further used for the synthesis of the hybrid structure with MWCNTs. In Fig. 1(c), the diffraction peaks at 25.3° and 42.6° are reflections from (002) and (100) planes, belonging to hexagonal planes of graphite for carbon nanotubes (JCPDS No. 41-1487). The MWCNTs are highly pure with a lower count of graphite. The XRD of the MWCNT@V_2CT_x [Fig. 1(d)] reveals the existence of the two phases in the composite. The (002) peak of V_2CT_x remains at a similar 2Θ, which is a slight shift toward the lower angle, i.e., 2Θ = 8.24°. Additionally, the non-out-of-plane MXene reflections are visible. The appearance of a broad peak at 2Θ = 22.14° represents the presence of multiwall carbon nanotubes in the hybrid structure.[57,58]

Scanning electron microscopy (SEM) was carried out for the morphological analysis (Fig. 2). Figure 2(a) reveals the bulk V_2AlC MAX phase particles. After the selective removal of Al layers, the etched MXene has a typical accordion-like structure [Fig. 2(b)]; the inset shows a high-resolution image. This lamellar structure indicates the successful etching of the Al layers after the chemical etching treatment.[59,60] The cross-sectional SEM image of the MWCNT@V_2CT_x [Fig. 2(c)] shows that MWCNTs form a uniform coverage network around the surface of V_2CT_x MXene particles. This unique structure provides an enhanced conductive network to assist the accessibility of electrolyte ions for a better electrochemical activity, hence resulting in improved energy storage.[61–63] To further investigate the assembly of MWCNTs on MXene particles, the high-resolution transmission electron microscopy (HRTEM) of MXene, MWCNT, and MWCNT@V_2CT_x MXene was carried out. Figure 2(d) shows MXene sheets that are oriented along the basal plane, and the selective area electron diffraction pattern (SAED) data [inset, Fig. 2(d)] show that the pristine MXene possesses a regular hexagonal structure, as is also reported before.[19,64] Figure 2(f) illustrates that upon the addition of MWCNTs, MXene sheets keep their crystalline structure. The inner section represents the hexagonal structure of the MXene, whereas the outer ring corresponds to the characteristic of MWCNT.[65]

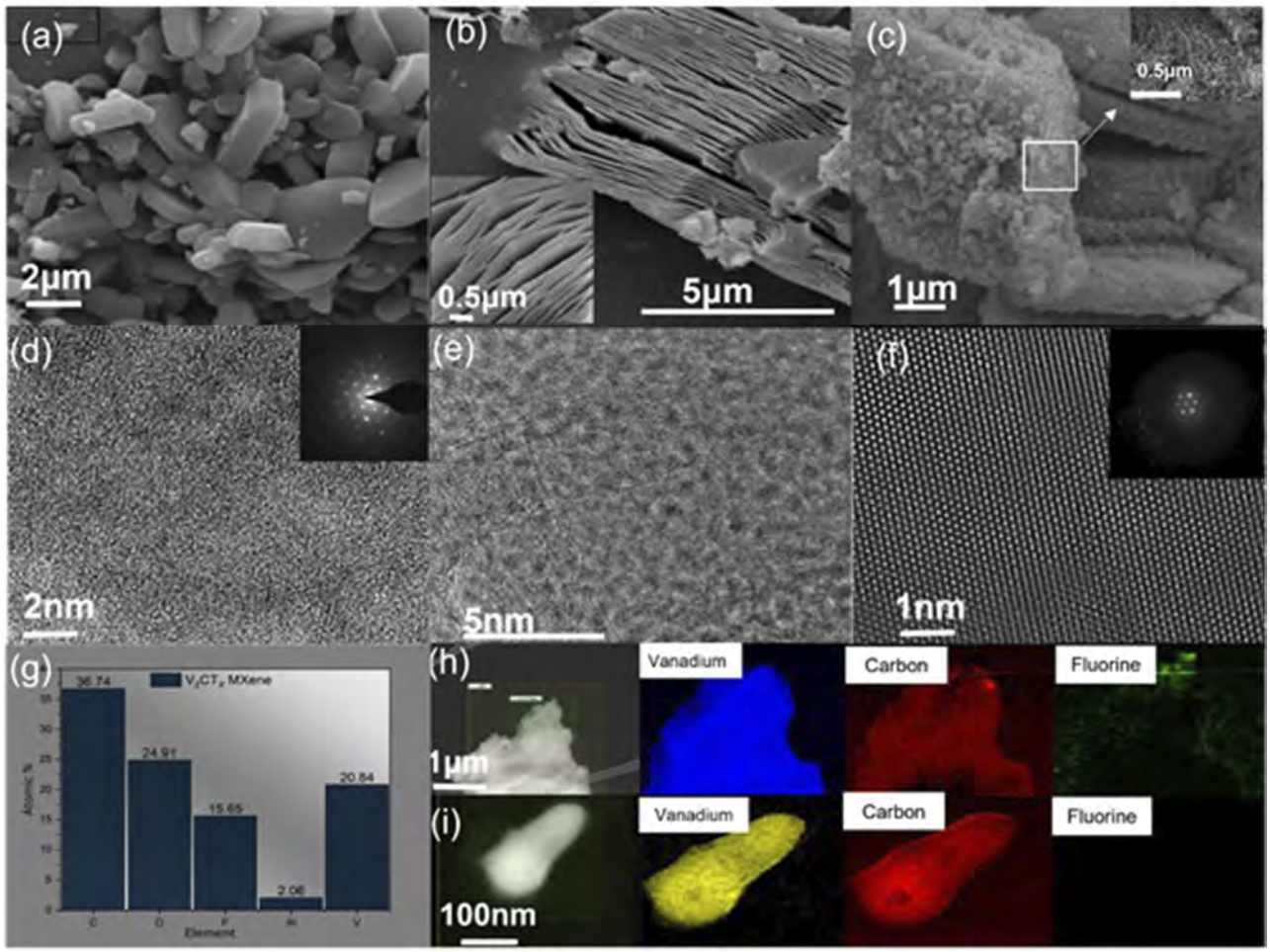

FIG. 2. (a)–(c) SEM micrographs of the V_2AlC MAX phase, V_2CT_x MXene, and MWCNT@V_2CT_x MXene, respectively; (d)–(f) HRTEM of MXene, MWCNT, and MWCNT@V_2CT_x MXene, respectively; (g) EDX of MXene; and (h)–(i) EELS mapping of MXene and MWCNT@V_2CT_x MXene, respectively.

The composition of as-synthesized V_2CT_x MXene was analyzed via energy dispersive spectroscopy (EDS) in SEM, shown in Fig. 2(g). The comparison of atomic percentages of the elements indicates that the as-prepared MXene has a small remaining Al (V:Al is ~10:1), which is due to the unetched MAX in agreement with XRD results [Fig. 2(a)]. Additionally, EDS revealed that the as-synthesized V_2CT_x MXene has more F than O, which is the result of the use of 50% HF and agrees with the previously reported results.[66,67] Because EDS does not quantify carbon accurately, we do not include carbon values. Figure 2(h) presents the elemental mapping of as-prepared MXene. The fluorine map in Fig. 2(h) indicates a higher concentration of F at the edges of V_2CT_x surface terminations originated as a result of HF etching. While in the mapping of MWCNT@V_2CT_x, these are shadowed by the carbon nanotubes, hence, the MWCNT forms a homogeneous network that increases the conductive channels between MXene layers for efficient charge transport and enhanced storage.[68]

The structural and phase transformations were investigated by collecting and analyzing Raman spectra (Fig. 3). The exfoliated MXenes are very sensitive to the Raman laser depending upon the etching route and the surface terminations.[67–70] Typical ω_1 vibrational mode (associated with V–Al bonding) is present in the V_2AlC MAX phase [Fig. 3(a)] that eventually disappears in the exfoliated MXene, and new peaks appear in the range of 280–700 cm^{-1} [Fig. 3(b)]. The vanishing of ω_1 in V_2CT_x MXene describes the effective etching of Al and the formation of an exfoliated MXene structure. A new peak that appears at a frequency of 284 cm^{-1} E_1g is ascribed to the enhanced interlayer spacing in V_2CT_x MXene as compared to its MAX phase precursor, representing the in-plane vibration of V-atoms.[71] The peaks at 406, 520, and 692 cm^{-1} represent the active vibrational modes of surface-terminated MXene.[2,72] Champagne *et al.* reported that the peak at 406 cm^{-1} is due to $V_2C(OH)_2$ representing out-of-plane V-atom vibrational modes, while the remaining two peaks are due to the A_1g mode of MXene corresponding to V_2CF_x and $V_2CO(OH)_2$, respectively, confirming further the etching of MXene with the presence of –O, –OH, and –F surface terminations. The small deviation from the theoretical values is due to surface chemistry as these functional groups can considerably influence the V atom vibrations with both the D and G bands present at 1336 and 1569 cm^{-1}, respectively, in MWCNT along with 2D bands at higher frequency [Fig. 3(c)], representing high purity of MWCNT with lesser defects. The humps present at higher frequencies are due to the intrinsic defects associated with random stacking of MXene sheets.[67] In hybrid materials, i.e., MWCNT@V_2CT_x, further shifting of peaks is observed along with the broadening of peaks, which can be explained by weak covalent bonding of MWCNT over the surface of V_2CT_x MXene.[72–77]

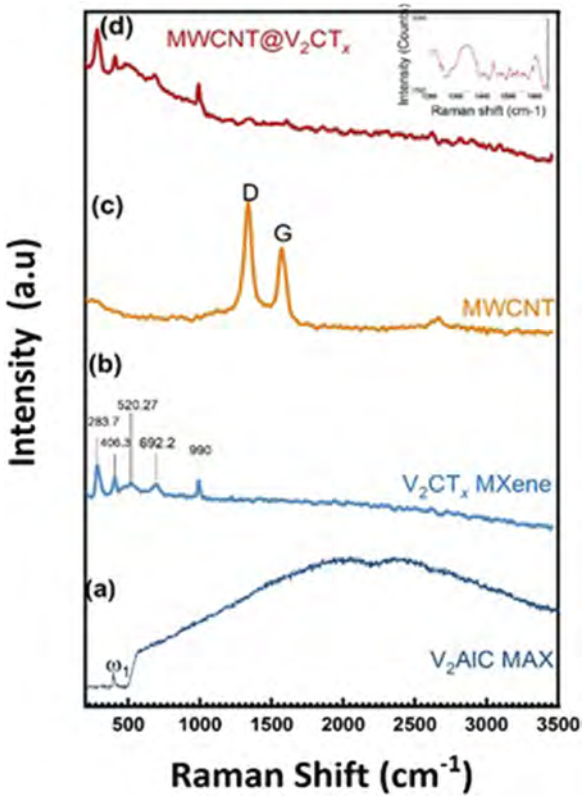

FIG. 3. Raman spectra of (a) the V_2AlC MAX phase, (b) V_2CT_x MXene, (c) MWCNT, and (d) MWCNT@V_2CT_x MXene.

The electrochemical tests [cyclic voltammetry (CV), GCD (galvanostatic charge-discharge), electrochemical impedance spectroscopy (EIS), and electrochemical cycling] were performed using the Gamry electrochemical workstation in a 1M KOH electrolyte. The Pt wire was used as a counter, while Ag/Ag Cl was used as the reference electrode and MWCNT@V_2CT_x was used as the working electrode in a three-electrode setup. The CV measurements of MWCNTs, V_2CT_x, and MWCNT@V_2CT_x at a scan rate of 200 mV s^{-1} over a potential window of –0.2–0.5 V are shown in Fig. 4(a). The better electrochemical performance and redox process in MWCNT@V_2CT_x compared to the pristine MXene was observed, which is a result of increased conductivity due to the introduction of MWCNTs. Figure 4(b) represents the CV curves for different CNTs: MXenes hybrids with weight ratios of 2:2, 1:2, 0.5:2, and 0.25:2, labeled, respectively as M1, M2, M3, and M4. The shape of these CV curves is significantly different from the porous carbon, which is rectangular owing to the double layer phenomenon.[78] The redox peaks suggest that the capacitance of these composites is mainly a pseudocapacitive based redox mechanism. An increase in CNT concentration results in an increased area under the curve, but after a certain limit, it starts to decrease again. Hence, by comparing the CV curves, we selected the M2 sample to carry on further electrochemical testing. Figure 4(c) represents the general trend of CV curves of the M2 hybrid structure measured at different scan rates ranging from 10–200 mV s^{-1}. The shape of the curves is maintained even at higher scan rates, revealing the fast reaction kinetics and durability of the electrode. The gravimetric capacitance [inset of Fig. 4(d)] gradually decreases with the increase in scan rate; however, at the same scan rate, the gravimetric capacitance of the hybrid structure is much greater compared to that of the pristine MXene and MWCNT. For instance, at 200 mV s^{-1}, the gravimetric capacitance of the hybrid structure is 576 F g^{-1}, of the pristine MXene is 230.5 F g^{-1}, and of MWCNT is 98.14 F g^{-1}. Electrostatic impedance spectroscopy of pristine and hybrid MXene was carried out [Fig. 4(d)] to study the

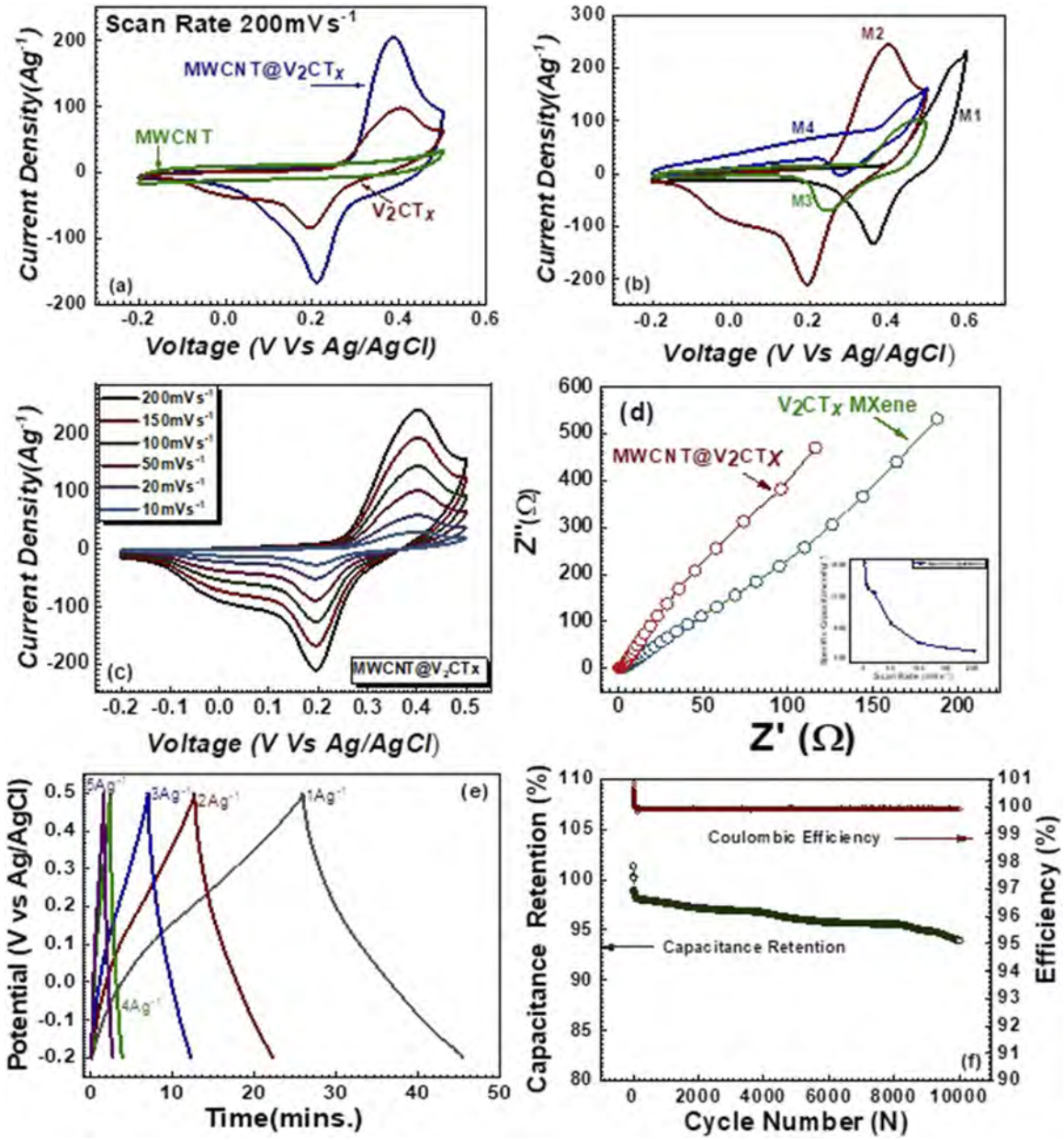

FIG. 4. (a) C–V of MWCNT, pristine, and MWCNT@V_2CT_x MXene at a scan rate of 200 mV s^{-1}. (b) C–V plots of various ratios of MWCNT@V_2CT_x at scan rates 200 mV s^{-1}. (c) C–V plots of M2 at different scan rates. (d) Comparison of EIS plots of pristine and M2 in 1 M KOH electrolyte; inset: specific capacitance vs scan rate graph of MWCNT@V_2CT_x MXene. (e) GCD plots at different current densities. (f) Capacitance retention (green) and coulombic efficiency (red) plots.

internal resistance. The fitted Nyquist plots represent the electrode impedance that includes the charge transfer resistance and internal series resistance at high frequencies. The Warburg impedance at low frequencies is less for MWCNT@V_2CT_x as compared to pristine MXene. The reason is the good hydrophilicity of MXene sheets and an improved conductivity due to the introduction of MWCNTs.[79] The improved electrical conductivity favors the rapid ion diffusion during the charge–discharge process by effectively decreasing the internal resistance and transportation of the electrolyte ions, hence resulting in the enhanced electrochemical performance of the hybrid material. The maximum specific capacitance of 1842 F g^{-1} was calculated from the CV curves at the scan rate of 2 mV s^{-1}. The nonlinear capacitive GCD curves at different current densities are represented in Fig. 4(e), revealing the pseudocapacitive nature of the

hybrid material. The following formula was used to calculate specific charge capacity:

$$Specific\ Charge\ Capacity = \frac{I \times \Delta t}{3.6 \times m}.$$

A maximum specific charge capacity of 62.5 A h g^{-1} was obtained at a current density of 1 A g^{-1}. The composite has a competitive energy density of 100.85 W h kg^{-1} with an admirable power density of 451 W kg^{-1}. The introduction of porous MWCNTs forms a homogeneous uniform network that increases the accessibility of active sites for fast ion diffusion. The cyclic performance was tested via galvanostatic charge–discharge at a current density of 10 A g^{-1}. It can be seen that the electrodes are stable up to 10 000 cycles with 94% capacitance retention capability, proving the higher rate capability of the hybrid material. The coulombic efficiency was tested at a current density of 1 A g^{-1} and was found to be 100% [Fig. 4(f)]. Keeping in view the enhanced performance, the hybrid material was tested over a wider potential range of −0.4–0.7 V (Fig. S1). The hybrid material has a larger area under the curve and possesses a gravimetric capacitance of 696 F g^{-1} @ 200 mV s^{-1}, and a maximum capacitance of 2386 F g^{-1} was achieved at the scan rate of 2 mV s^{-1}. The phenomenon of oxidation is prominent at a lower scan rate in this voltage window that might be due to the degradation of the electrolyte or the base material. However, at the higher scan rates, the electrode shows an outstanding performance due to enhanced conductive channels provided by MWCNTs homogeneous linkage.

A. Structures and electronic properties

Figure 5(a) depicts optimized structures of the V_2CT_x MXene (T = F/O) and (T = F, OH), respectively. Saturation of surface O* groups with hydrogen atoms (T = F and OH) results in a noticeable deformation in reference to the V_2CT_x MXene (T = F/O). In the latter structure, V_2CT_x MXene (T = F/O), oxygen and fluorine atoms reside at three-fold hollow sites over the V network at which the V–F and C–O distances amount to 1.847 and 2.000 Å; respectively. Likewise, the V–C distances feature two bond lengths, namely, 2.100 and 2.350 Å. V, C, O, and F atoms uniformly entail partial atomic charges (Mulliken) of 0.67, 0.48, −0.32, and 0.45*e*, respectively. Saturation of surface O* groups with the H atom results in a noticeable deformation, as portrayed in Fig. 5. In the top layer, fluorine atoms moved downward to accommodate the positive charge influx by V atoms. Vanadium atoms entail positive charges in the range of 0.55 and 0.81*e*; respectively. The variation in atomic charges throughout the structure reflects structural arrangements induced by OH* groups.

It was demonstrated recently that the charge extraction process in various MXenes can be enhanced by fine-tuning their work function values.[80] The computed work function of the V_2CT_x MXene (T = F/O) attains a value of 5.7 eV. This value drops to only 2.16 eV for the V_2CT_x MXene (T = F/OH). Thus, it is envisaged that the latter structure exhibited enhanced super capacitance performance than the V_2CT_x MXene (T = F/O). It will be insightful to assess the influence of the relative loads of the T_x functional groups on the variation of the work function with the inclusion of a solvent environment. The presence of the vanadium atom in these MXenes renders them metallic character where all states around the Fermi level are filled. Using the LST/QST (linear strain triangle/quadratic strain triangle) method, we found that water dissociation over the V_2CT_x MXene (T = F/O) incurs an accessible activation energy of 1.2 eV. Thus, hydroxylation reactions are expected to readily transform V_2CT_x Mxene (T = F/O) into V_2CT_x MXene (T = F/OH). The addition of an H atom to the O* group in the V_2CT_x MXene (T = F/O) is highly exothermic by 2.39 eV and does not encounter an activation barrier.

Figure 5(b) shows the optimized structure of the CNT-V_2CT_x MXene T = F/O structure. The outer carbon atom of the considered CNT was terminated with hydrogen atoms. The CNT configurations reside 2.930 Å above the MXene. Carbon atoms in the CNT hold minimal positive charges in the range 0.0–0.04*e*, revealing a very minor interaction. As demonstrated in Fig. 5(c), the CNT-V_2CT_x MXene (T = F/O) structure retains a metallic character owing to the d states of vanadium atoms. As expected, adding the CNT does not alter the main structural and electronic features of the neat V_2CT_x MXene (T = F/O) structure, in agreement with SAED in inset of Fig. 2(f) where MXene retained their hexagonal structure and a characteristic outer ring appears due to MWCNT. Nevertheless, improved capacitance can be attributed to increased

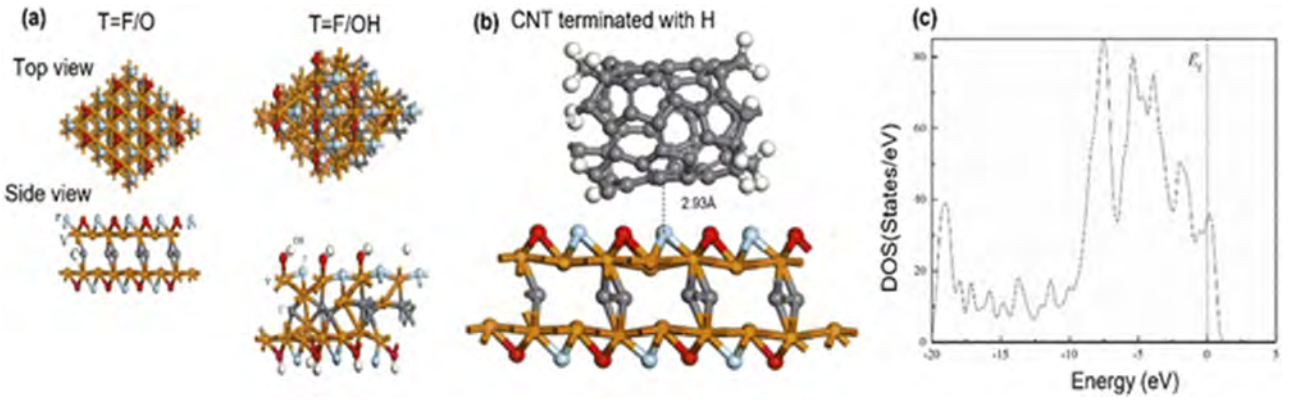

FIG. 5. (a) Optimized structures of the two considered V_2CT_x MXene. (b) Optimized structures of the two considered CNT-V_2CT_x MXene (T = F/O). (c) Density of state curve for the CNT-V_2CT_x MXene (T = F/O) structure. The dashed line represents the Fermi level.

electrical conductivity of the CNT-MXene hybrid structure due to MWCNTs where the CNTs provide a conductive path rather than influencing the intra-particle dynamics.[59] In addition, higher electrical conductivity of the CNT-MXene hybrid was observed during electrochemical experiments in agreement with the 0 eV Fermi level for conduction in Fig. 5(c).

III. EXPERIMENTAL SECTION

A. Preparation of MXene

The wet chemical etching route was used for the synthesis of MXene. 1 g of V_2AlC MAX (300 mesh) powder was treated with 50% hydrofluoric acid in a Teflon bottle for 72 h while stirring at 400 rpm at room temperature. The chemically etched powder was washed several times with de-ionized (DI) water and centrifuged at 3000 rpm/5 min per cycle until the PH of the supernatant reached above 6. The solution was then vacuum filtered and dried under vacuum at 50 °C for 24 h.

B. Synthesis of MWCNT@V_2CT_x composite

Cetyl Trimethyl Ammonium Bromide (CTAB) grafted MWCNT was prepared by dissolving 2 mg of CTAB in 20 ml DI water via magnetic stirring to achieve a uniform aqueous solution. After that, MWCNTs were dispersed in CTAB solution via probe sonication to a concentration of 0.5 mg/ml. Briefly, 20 ml of CTAB grafted MWCNT solution was added drop-wise to 50 ml (0.4 mg/ml) of V_2CT_x solution. The resultant mixture was probe sonicated for 10 min followed by vacuum filtration and vacuum drying at 50 °C overnight to get a composite material. In a similar manner, different weight ratios of CNT:MXene (1:1, 1:2, 0.5:2, and 0.25:2) composites, labeled as M1, M2, M3, and M4, were prepared for the thorough study of the effect of CNTS.

C. Material characterization

The crystal structure and phase identification were carried out using a powder x-ray diffraction (DRON-8) diffractometer equipped with the Cu K-α (λ 0.154 nm) source in the 2Θ range of 3°–70°. A Hitachi s-4800 FEG (field emission gun) scanning electron microscope was used for the study of surface morphology. Transmission electron microscopy (TEM) analysis was used to further investigate the morphology. The high-resolution images were acquired on Titan 60–300 from Thermo Fischer Scientific equipped with an imaging Cs-corrector and working at 300 kV. Elementary mappings were performed using the scanning TEM (STEM) mode associated with an energy-dispersive x-ray spectroscopy (EDS) detector and an electron energy loss spectroscopy (EELS) detector (Gatan). Raman spectra were obtained using a Thermo Renishaw with laser excitation λ = 532 nm of the He–Ne laser.

D. Electrochemical measurements

The electrochemical testing of the as-synthesized samples was carried out in the 1M KOH electrolyte with the Gamry 1010B Potentiostat workstation. The working electrode was prepared by mixing the as-synthesized MWCNT@V_2CT_x composite with 5 wt. % polyvinylidene fluoride (PVDF) binder dissolved in N-methyl 2-pyrrolidone (NMP) in a 90:10 ratio. The prepared slurry was coated on the 1 × 1 cm^2 Ni foam current collector and then vacuum-dried at 60 °C for 24 h. The dried electrodes were pressed under 5–10 MPa pressure for 10 s. The prepared electrodes were dipped in 1 M KOH overnight before performing the cyclic voltammetry. All the tests were conducted in a three-electrode Swaglock cell. Platinum wire was used as a counter electrode, while Ag/AgCl in 3.5 M KCl was used as a reference electrode. The CV voltammograms were recorded in the voltage ranges of −0.2–0.5 V and −0.4–0.7 V under a scan rate range of 2–200 mV s^{-1}. The EIS was acquired at the open circuit potential (OCP) in a frequency range of 20 kHz to 10 mHz using a sinusoidal signal of 10 mV.

The following formulas were used to calculate the gravimetric capacitance:

From CV,

$$C = \int I(V)dV/mV\Delta V,$$

where I is the current, m is the active mass of the electrode, V is the scan rate, and ΔV is the potential window.

From GCD,

$$C = I \int (1/V(t))dt,$$

where I is the constant current density and V is the working potential as a function of time.

The specific capacity was calculated from GCD using the following formula:

$$Specific\ charge\ capacity = \frac{I \times \Delta t}{3.6 \times m}.$$

The energy density and power density of the MWCNT@V2CT$_x$ MXene were calculated using the following formulas:

$$E = \frac{\frac{1}{2}CV^2}{3.6},$$

$$P = \frac{E}{\Delta t} \times 3\,600.$$

IV. CONCLUSION

In summary, we have demonstrated a simple method for the synthesis of 2D V_2CT_x MXene and its composite with MWCNT. The MWCNTs were used to enhance the electrical conductivity of MXene sheets by forming a uniform network between the V_2CT_x MXene multi-layer particles. Hence, the electrode material exhibited enhanced super-capacitive performance with a maximum gravimetric capacitance of 1842 F g^{-1}. The specific charge capacity was found to be 62.5 A h g^{-1}. The introduction of MWCNTs not only increased interlayer spacing but also improved the electrical conductivity. The capacitive retention was found to be 94% until the 10 000 cycle that shows much higher stability of the composite. Hence, the MWCNT@V_2CT_x composite materials are promising candidates for pseudocapacitive energy storage devices.

SUPPLEMENTARY MATERIAL

See the supplementary material for experimental details of electrochemical testing at higher voltage windows.

ACKNOWLEDGMENTS

The authors thank the Higher Education Commission (HEC) of Pakistan for providing research funding under Project No. 20-14784/NRPU/R & D/HEC/2021.

AUTHOR DECLARATIONS

Conflict of Interest

The authors have no conflicts to disclose.

Author Contributions

S.A.Z. performed experimentation and paper writing; B.A. helped in data analysis and paper writing; F.R. and M.Z.I. helped in HRTEM and elemental analysis; M.A.T. performed DFT analysis; and S.R. conceived the research concept, helped in paper writing, and supervised the complete project.

DATA AVAILABILITY

The data that support the findings of this study are available within the article and its supplementary material.

REFERENCES

[1] J. Zhang, T. Xu, Y. Cong, Y. Zhang, X. Li, Z. Dong, Y. Li, G. Yuan, J. Zhang, and Z. Cui, "Improved rate performance and cycling stability of graphitized mesoporous carbon as anode materials for lithium-ion batteries," J. Mater. Sci. **54**(1), 648–658 (2019).

[2] Y. Guan, S. Jiang, Y. Cong, J. Wang, Z. Dong, Q. Zhang, G. Yuan, Y. Li, and X. Li, "A hydrofluoric acid-free synthesis of 2D vanadium carbide (V_2C) MXene for supercapacitor electrodes," 2D Mater. **7**(2), 025010 (2020).

[3] T. Kim, W. Song, D.-Y. Son, L. K. Ono, and Y. Qi, "Lithium-ion batteries: Outlook on present, future, and hybridized technologies," J. Mater. Chem. A **7**(7), 2942–2964 (2019).

[4] C. Wang, S. Wei, S. Chen, D. Cao, and L. Song, "Delaminating vanadium carbides for zinc-ion storage: Hydrate precipitation and H^+/Zn^{2+} Co-action mechanism," Small Methods **3**(12), 1900495 (2019).

[5] R. Schmuch, R. Wagner, G. Hörpel, T. Placke, and M. Winter, "Materials for automotive batteries: Perspective on performance and cost of lithium-based rechargeable batteries," Nat. Energy **3**, 267–278 (2017).

[6] Z. Xing, S. Wang, A. Yu, and Z. Chen, "Aqueous intercalation-type electrode materials for grid-level energy storage: Beyond the limits of lithium and sodium," Nano Energy **50**, 229–244 (2018).

[7] P. Huang, C. Lethien, S. Pinaud, K. Brousse, R. Laloo, V. Turq, and P. Simon, "On-chip and freestanding elastic carbon films for micro-supercapacitors," Science **351**(6274), 691–695 (2016).

[8] A. Noori, M. F. El-Kady, M. S. Rahmanifar, R. B. Kaner, and M. F. Mousavi, "Towards establishing standard performance metrics for batteries, supercapacitors, and beyond," Chem. Soc. Rev. **48**(5), 1272–1341 (2019).

[9] Y. Shao, M. F. El-Kady, J. Sun, Y. Li, Q. Zhang, M. Zhu, and R. B. Kaner, "Design and mechanisms of asymmetric supercapacitors," Chem. Rev. **118**(18), 9233–9280 (2018).

[10] X. Wang, T. S. Mathis, K. Li, Z. Lin, L. Vlcek, T. Torita, and Y. Gogotsi, "Influences from solvents on charge storage in titanium carbide MXenes," Nat. Energy **4**(3), 241–248 (2019).

[11] D. Feng, T. Lei, M. R. Lukatskaya, J. Park, Z. Huang, M. Lee, and Z. Bao, "Robust and conductive two-dimensional metal–organic frameworks with exceptionally high volumetric and areal capacitance," Nat. Energy **3**(1), 30–36 (2018).

[12] D. P. Dubal, N. R. Chodankar, D.-H. Kim, and P. Gomez-Romero, "Towards flexible solid-state supercapacitors for smart and wearable electronics," Chem. Soc. Rev. **47**(6), 2065–2129 (2018).

[13] C. Choi, D. S. Ashby, D. M. Butts, R. H. DeBlock, Q. Wei, J. Lau, and B. Dunn, "Achieving high energy density and high power density with pseudocapacitive materials," Nat. Rev. Mater. **5**(1), 5–19 (2020).

[14] H. Li, T. Lv, H. Sun, G. Qian, N. Li, Y. Yao, and T. Chen, "Ultra stretchable and superior healable supercapacitors based on a double cross-linked hydrogel electrolyte," Nat. Commun. **10**(1), 536 (2019).

[15] Z. Wang, H. Su, F. Liu, X. Chu, C. Yan, B. Gu, and W. Yang, "Establishing highly-efficient surface faradaic reaction in flower-like $NiCo_2O_4$ nano-/micro-structures for next-generation supercapacitors," Electrochim. Acta **307**, 302–309 (2019).

[16] H. Su, H. Huang, H. Zhang, X. Chu, B. Zhang, B. Gu, and W. Yang, "In situ direct method to massively prepare hydrophilic porous carbide-derived carbons for high-performance supercapacitors," ACS Appl. Energy Mater. **1**(8), 3544–3553 (2018).

[17] Z. Lei, L. Liu, H. Zhao, F. Liang, S. Chang, L. Li, and Y. Lei, "Nanoelectrode design from microminiaturized honeycomb monolith with ultrathin and stiff nano scaffold for high-energy micro-supercapacitors," Nat. Commun. **11**(1), 299 (2020).

[18] H. Zhang, H. Su, L. Zhang, B. Zhang, F. Chun, X. Chu, and W. Yang, "Flexible supercapacitors with high areal capacitance based on hierarchical carbon tubular nanostructures," J. Power Sources **331**, 332–339 (2016).

[19] M. Naguib, M. Kurtoglu, V. Presser, J. Lu, J. Niu, M. Heon, and M. W. Barsoum, "Two-dimensional nanocrystals: Two-dimensional nanocrystals produced by exfoliation of Ti_3AlC_2 (Adv. Mater. 37/2011)," Adv. Mater. **23**(37), 4207 (2011).

[20] Y. Gogotsi and B. Anasori, "The rise of MXenes," ACS Nano **13**, 8491 (2019).

[21] M. W. Barsoum, "The $M_{N+1}AX_N$ phases: A new class of solids: Thermodynamically stable nanolaminates," Prog. Solid State Chem. **28**, 201–281 (2000).

[22] B.-M. Jun, S. Kim, J. Heo, C. M. Park, N. Her, M. Jang, Y. Huang, J. Han, and Y. Yoon, "Review of MXenes as new nanomaterials for energy storage/delivery and selected environmental applications," Nano Res. **12**, 471–487 (2019).

[23] L. Verger, V. Natu, M. Carey, and M. W. Barsoum, "MXenes: An introduction of their synthesis, select properties, and applications," Trends Chem. **1**(7), 656–669 (2019).

[24] B. Anasori, M. R. Lukatskaya, and Y. Gogotsi, "2D metal carbides and nitrides (MXenes) for energy storage," Nat. Rev. Mater. **2**, 16098 (2017).

[25] J. Pang, R. G. Mendes, A. Bachmatiuk, L. Zhao, H. Q. Ta, T. Gemming, H. Liu, Z. Liu, and M. H. Rummeli, "Applications of 2D MXenes in energy conversion and storage systems," Chem. Soc. Rev. **48**, 72–133 (2019).

[26] M. Alhabeb, K. Maleski, B. Anasori, P. Lelyukh, L. Clark, S. Sin, and Y. Gogotsi, "Guidelines for synthesis and processing of two-dimensional titanium carbide ($Ti_3C_2T_x$ MXene)," Chem. Mater. **29**, 7633–7644 (2017).

[27] P. Eklund, M. Beckers, U. Jansson, H. Högberg, and L. Hultman, "The $M_{n+1}AX_n$ phases: Materials science and thin-film processing," Thin Solid Films **518**, 1851–1878 (2010).

[28] G. Deysher, C. E. Shuck, K. Hantanasirisakul, N. C. Frey, A. C. Foucher, K. Maleski, and Y. Gogotsi, "Synthesis of Mo_4VAlC_4 MAX phase and two-dimensional Mo_4VC_4 MXene with five atomic layers of transition metals," ACS Nano **14**(1), 204–217 (2019).

[29] B. C. Wyatt, A. Rosenkranz, and B. Anasori, "2D MXenes: Tunable mechanical and tribological properties," Adv. Mater. **33**(17), 2007973 (2021).

[30] Z. Li, L. Wang, D. Sun, Y. Zhang, B. Liu, Q. Hu, and A. Zhou, "Synthesis and thermal stability of two-dimensional carbide MXene Ti_3C_2," Mater. Sci. Eng. B **191**, 33–40 (2015).

[31] F. Liu, A. Zhou, J. Chen, H. Zhang, J. Cao, L. Wang, and Q. Hu, "Preparation and methane adsorption of two-dimensional carbide Ti_2C," Adsorption **22**(7), 915–922 (2016).

[32]D. Sun, M. Wang, Z. Li, G. Fan, L.-Z. Fan, and A. Zhou, "Two-dimensional Ti_3C_2 as anode material for Li-ion batteries," Electrochem. Commun. **47**, 80–83 (2014).
[33]A. Iqbal, J. Kwon, M.-K. Kim, and C. M. Koo, "MXenes for electromagnetic interference shielding: Experimental and theoretical perspectives," Mater. Today Adv. **9**, 100124 (2021).
[34]K. R. G. Lim, A. D. Handoko, S. K. Nemani, B. Wyatt, H.-Y. Jiang, J. Tang, and Z. W. Seh, "Rational design of two-dimensional transition metal carbide/nitride (MXene) hybrids and nanocomposites for catalytic energy storage and conversion," ACS Nano **14**(9), 10834–10864 (2020).
[35]G. Ding, K. Zeng, K. Zhou, Z. Li, Y. Zhou, Y. Zhai, and S. T. Han, "Configurable multi-state non-volatile memory behaviors in Ti_3C_2 nanosheets," Nanoscale **11**(15), 7102–7110 (2019).
[36]S. Gul, M. I. Serna, S. A. Zahra, N. Arif, M. Iqbal, D. Akinwande, and S. Rizwan, "Un-doped and Er-adsorbed layered Nb_2C MXene for efficient hydrazine sensing application," Surf. Interfaces **24**, 101074 (2021).
[37]M. Iqbal, J. Fatheema, Q. Noor, M. Rani, M. Mumtaz, R.-K. Zheng, and S. Rizwan, "Co-existence of magnetic phases in two-dimensional MXene," Mater. Today Chem. **16**, 100271 (2020).
[38]Q. Noor, S. A. Zahra, M. I. Serna, C. K. Abuoudah, M. Z. Iqbal, D. Akinwande, and S. Rizwan, "Silicon carbide-assisted co-existence of magnetic phases in well-optimized Ti_3SiC_2-etched MXene," Ceram. Int. **46**(17), 27419–27425 (2020).
[39]Z. U. D. Babar, R.-K. Zheng, M. Mumtaz, and S. Rizwan, "Magneto-transport of mechanically-pressed niobium carbide (Nb_2C) distorted MXene," Mater. Lett. **285**, 129210 (2021).
[40]M. Fatima, J. Fatheema, N. B. Monir, A. H. Siddique, B. Khan, A. Islam, and S. Rizwan, "Nb-doped MXene with enhanced energy storage capacity and stability," Front. Chem. **8**, 168 (2020).
[41]Z. U. Din Babar, J. Fatheema, N. Arif, M. S. Anwar, S. Gul, M. Iqbal, and S. Rizwan, "Magnetic phase transition from paramagnetic in Nb_2AlC-MAX to superconductivity-like diamagnetic in Nb_2C-MXene: An experimental and computational analysis," RSC Adv. **10**(43), 25669–25678 (2020).
[42]J. Fatheema, M. Fatima, N. B. Monir, S. A. Khan, and S. Rizwan, "A comprehensive computational and experimental analysis of stable ferromagnetism in layered 2D Nb-doped Ti_3C_2 MXene," Physica E **124**, 114253 (2020).
[43]M. A. Iqbal, A. Tariq, A. Zaheer, S. Gul, S. I. Ali, M. Z. Iqbal, and S. Rizwan, "Ti_3C_2-MXene/bismuth ferrite nanohybrids for efficient degradation of organic dyes and colorless pollutants," ACS omega **4**(24), 20530–20539 (2019).
[44]S. Rafiq, S. Awan, R.-K. Zheng, Z. Wen, M. Rani, D. Akinwande, and S. Rizwan, "Novel room-temperature ferromagnetism in Gd-doped 2-dimensional $Ti_3C_2T_x$ MXene semiconductor for spintronics," J. Magn. Magn. Mater. **497**, 165954 (2020).
[45]J. Hu, B. Xu, C. Ouyang, S. A. Yang, and Y. Yao, "Investigations on V_2C and V_2CX_2 (X = F, OH) monolayer as a promising anode material for Li ion batteries from first-principles calculations," J. Phys. Chem. C **118**(42), 24274–24281 (2014).
[46]D. Sun, Q. Hu, J. Chen, X. Zhang, L. Wang, Q. Wu, and A. Zhou, "Structural transformation of MXene (V_2C, Cr_2C, and Ta_2C) with O groups during lithiation: A first-principles investigation," ACS Appl. Mater. Interfaces **8**(1), 74–81 (2016).
[47]Q. Shan, X. Mu, M. Alhabeb, C. E. Shuck, D. Pang, X. Zhao, and Y. Dall'Agnese, "Two-dimensional vanadium carbide (V_2C) MXene as electrode for supercapacitors with aqueous electrolytes," Electrochem. Commun. **96**, 103–107 (2018).
[48]B. Yan, C. Lu, P. Zhang, J. Chen, W. He, W. Tian, and Z. Sun, "Oxygen/sulfur decorated 2D MXene V_2C for promising lithium ion battery anodes," Mater. Today Commun. **22**, 100713 (2020).
[49]F. Liu, Y. Liu, X. Zhao, K. Liu, H. Yin, and L. Z. Fan, "Prelithiated V_2C MXene: A high-performance electrode for hybrid magnesium/lithium-ion batteries by ion cointercalation," Small **16**(8), 1906076 (2020).
[50]R. Venkatkarthick, N. Rodthongkum, X. Zhang, S. Wang, P. Pattananuwat, Y. Zhao, and J. Qin, "Vanadium-based oxide on two-dimensional vanadium carbide MXene (V_2O_x@V_2CT_x) as cathode for rechargeable aqueous zinc-ion batteries," ACS Appl. Energy Mater. **3**(5), 4677–4689 (2020).
[51]C. Zhan, W. Sun, P. R. C. Kent, M. Naguib, Y. Gogotsi, and D.-e. Jiang, "Computational screening of MXene electrodes for pseudocapacitive energy storage," J. Phys. Chem. C **123**(1), 315–321 (2018).
[52]J. M. Goff, F. Marques dos Santos Vieira, N. D. Keilbart, Y. Okada, and I. Dabo, "Predicting the pseudocapacitive windows for MXene electrodes with voltage-dependent cluster expansion models," ACS Appl. Energy Mater. **4**(4), 3151–3159 (2021).
[53]N. Keilbart, Y. Okada, A. Feehan, S. I. Higai, and I. Dabo, "Quantum-continuum simulation of the electrochemical response of pseudocapacitor electrodes under realistic conditions," Phys. Rev. B **95**(11), 115423 (2017).
[54]W. Zhang, J. Peng, W. Hua, Y. Liu, J. Wang, Y. Liang, and S. L. Chou, "Architecting amorphous vanadium oxide/MXene nanohybrid via tunable anodic oxidation for high-performance sodium-ion batteries," Adv. Energy Mater. **11**, 2100757 (2021).
[55]X. Xie, M.-Q. Zhao, B. Anasori, K. Maleski, C. E. Ren, J. Li, and Y. Gogotsi, "Porous heterostructured MXene/carbon nanotube composite paper with high volumetric capacity for sodium-based energy storage devices," Nano Energy **26**, 513–523 (2016).
[56]A. VahidMohammadi, A. Hadjikhani, S. Shahbazmohamadi, and M. Beidaghi, "Two-dimensional vanadium carbide (MXene) as a high-capacity cathode material for rechargeable aluminum batteries," ACS Nano **11**(11), 11135–11144 (2017).
[57]W. Zhang, H. Jin, G. Chen, and J. Zhang, "Sandwich-like N-doped carbon nanotube@Nb_2C MXene composite for high performance alkali ion batteries," Ceram. Int. **47**, 20610 (2021).
[58]P. Yan, R. Zhang, J. Jia, C. Wu, A. Zhou, J. Xu, and X. Zhang, "Enhanced supercapacitive performance of delaminated two-dimensional titanium carbide/carbon nanotube composites in alkaline electrolyte," J. Power Sources **284**, 38–43 (2015).
[59]M.-Q. Zhao, C. E. Ren, Z. Ling, M. R. Lukatskaya, C. Zhang, K. L. Van Aken, and Y. Gogotsi, "Flexible MXene/carbon nanotube composite paper with high volumetric capacitance," Adv. Mater. **27**(2), 339–345 (2015).
[60]Y. Liu, W. Wang, Y. Ying, Y. Wang, and X. Peng, "Binder-free layered Ti_3C_2/CNTs nanocomposite anodes with enhanced capacity and long-cycle life for lithium-ion batteries," Dalton Trans. **44**(16), 7123–7126 (2015).
[61]Q. Cheng, J. Tang, J. Ma, H. Zhang, N. Shinya, and L.-C. Qin, "Graphene and carbon nanotube composite electrodes for supercapacitors with ultra-high energy density," Phys. Chem. Chem. Phys. **13**(39), 17615–17624 (2011).
[62]X.-M. Liu, Z. d. Huang, S. w. Oh, B. Zhang, P.-C. Ma, M. M. F. Yuen, and J.-K. Kim, "Carbon nanotube (CNT)-based composites as electrode material for rechargeable Li-ion batteries: A review," Compos. Sci. Technol. **72**(2), 121–144 (2012).
[63]B. J. Landi, M. J. Ganter, C. D. Cress, R. A. DiLeo, and R. P. Raffaelle, "Carbon nanotubes for lithium ion batteries," Energy Environ. Sci. **2**(6), 638–654 (2009).
[64]L. Kong, X. Yin, X. Yuan, Y. Zhang, X. Liu, L. Cheng, and L. Zhang, "Electromagnetic wave absorption properties of graphene modified with carbon nanotube/poly(dimethyl siloxane) composites," Carbon **73**, 185–193 (2014).
[65]O. Mashtalir, M. Naguib, V. N. Mochalin, Y. Dall'Agnese, M. Heon, M. W. Barsoum, and Y. Gogotsi, "Intercalation and delamination of layered carbides and carbonitrides," Nat. Commun. **4**(1), 1716 (2013).
[66]J. Chen, K. Chen, D. Tong, Y. Huang, J. Zhang, J. Xue, and T. Chen, "CO_2 and temperature dual responsive 'Smart' MXene phases," Chem. Commun. **51**(2), 314–317 (2015).
[67]A. Champagne, L. Shi, T. Ouisse, B. Hackens, and J.-C. Charlier, "Electronic and vibrational properties of V_2C-based MXenes: From experiments to first-principles modeling," Phys. Rev. B **97**(11), 115439 (2018).
[68]R. Li, L. Zhang, L. Shi, and P. Wang, "MXene Ti_3C_2: An effective 2D light-to-heat conversion material," ACS Nano **11**(4), 3752–3759 (2017).
[69]M. Naguib, J. Halim, J. Lu, K. M. Cook, L. Hultman, Y. Gogotsi, and M. W. Barsoum, "New two-dimensional niobium and vanadium carbides as promising materials for Li-ion batteries," J. Am. Chem. Soc. **135**(43), 15966–15969 (2013).
[70]Q. Jiang, Y. Lei, H. Liang, K. Xi, C. Xia, and H. N. Alshareef, "Review of MXene electrochemical microsupercapacitors," Energy Storage Mater. **27**, 78–95 (2020).
[71]E. Lee, A. VahidMohammadi, Y. S. Yoon, M. Beidaghi, and D.-J. Kim, "Two-dimensional vanadium carbide MXene for gas sensors with ultrahigh sensitivity toward nonpolar gases," ACS Sens. **4**(6), 1603–1611 (2019).
[72]M. Wu, B. Wang, Q. Hu, L. Wang, and A. Zhou, "The synthesis process and thermal stability of V_2C MXene," Materials **11**(11), 2112 (2018).
[73]P. Kuang, M. He, B. Zhu, J. Yu, K. Fan, and M. Jaroniec, "0D/2D NiS_2/V-MXene composite for electrocatalytic H_2 evolution," J. Catal. **375**, 8–20 (2019).

[74]F. Ming, H. Liang, W. Zhang, J. Ming, Y. Lei, A.-H. Emwas, and H. N. Alshareef, "Porous MXenes enable high performance potassium ion capacitors," Nano Energy **62**, 853–860 (2019).
[75]S. Cao, B. Shen, T. Tong, J. Fu, and J. Yu, "2D/2D heterojunction of ultrathin MXene/Bi_2WO_6 nanosheets for improved photocatalytic CO_2 reduction," Adv. Funct. Mater. **28**(21), 1800136 (2018).
[76]Z. Wang, H. Kim, and H. N. Alshareef, "Oxide thin-film electronics using all-MXene electrical contacts," Adv. Mater. **30**(15), 1706656 (2018).
[77]J. Li, N. Kurra, M. Seredych, X. Meng, H. Wang, and Y. Gogotsi, "Bipolar carbide-carbon high voltage aqueous lithium-ion capacitors," Nano Energy **56**, 151–159 (2019).
[78]H. Sun, X. You, J. Deng, X. Chen, Z. Yang, J. Ren, and H. Peng, "Novel graphene/carbon nanotube composite fibers for efficient wire-shaped miniature energy devices," Adv. Mater. **26**(18), 2868–2873 (2014).
[79]Y. Dall'Agnese, P. Rozier, P. L. Taberna, Y. Gogotsi, and P. Simon, "Capacitance of two-dimensional titanium carbide (MXene) and MXene/carbon nanotube composites in organic electrolytes," J. Power Sources **306**, 510–515 (2016).
[80]A. Agresti, A. Pazniak, S. Pescetelli, A. Di Vito, D. Rossi, A. Pecchia, and A. Di Carlo, "Titanium-carbide MXenes for work function and interface engineering in perovskite solar cells," Nat. Mater. **18**(11), 1228–1234 (2019).